Research Paper

UTMD-Promoted Co-Delivery of Gemcitabine and miR-21 Inhibitor by Dendrimer-Entrapped Gold Nanoparticles for Pancreatic Cancer Therapy

Lizhou Lin[1*], Yu Fan[2*], Feng Gao[1], Lifang Jin[1], Dan Li[2], Wenjie Sun[2], Fan Li[1], Peng Qin[4], Qiusheng Shi[1✉], Xiangyang Shi[2, 3✉], Lianfang Du[1✉]

1. Department of Ultrasound, Shanghai General Hospital, Shanghai Jiaotong University School of Medicine, Shanghai 200080, P. R. China
2. College of Chemistry, Chemical Engineering and Biotechnology, Donghua University, Shanghai 201620, China
3. CQM-Centro de Química da Madeira, Universidade da Madeira, Campus da Penteada, 9000-390 Funchal, Portugal
4. Department of Instrument Science and Engineering, Shanghai Jiao Tong University, Shanghai, 201108, China

* Co-first Authors, contributed equally to this work

✉ Corresponding author: E-mail: dulf_sh@163.com (L. Du), sqs19631989@163.com (Q. Shi) and xshi@dhu.edu.cn (X. Shi)

Abstract

Conventional chemotherapy of pancreatic cancer (PaCa) suffers the problems of low drug permeability and inherent or acquired drug resistance. Development of new strategies for enhanced therapy still remains a great challenge. Herein, we report a new ultrasound-targeted microbubble destruction (UTMD)-promoted delivery system based on dendrimer-entrapped gold nanoparticles (Au DENPs) for co-delivery of gemcitabine (Gem) and miR-21 inhibitor (miR-21i).

Methods: In this study, Gem-Au DENPs/miR-21i was designed and synthesized. The designed polyplexes were characterized *via* transmission electron microscopy (TEM), Gel retardation assay and dynamic light scattering (DLS). Then, the optimum exposure parameters were examined by an ultrasound exposure platform. The cellular uptake, cytotoxicity and anticancer effects *in vitro* were analyzed by confocal laser microscopy, spectra microplate reader, flow cytometry and a chemiluminescence imaging system. Lastly, the anticancer effects *in vivo* were evaluated by contrast-enhanced ultrasound (CEUS), hematoxylin and eosin (H&E) staining, TUNEL staining and comparison of tumor volume.

Results: The results showed that the Gem-Au DENPs/miR-21i can be uptake by cancer cells and the cellular uptake was further facilitated by UTMD with an ultrasound power of 0.4 W/cm^2 to enhance the cell permeability. Further, the co-delivery of Gem and miR-21i with or without UTMD treatment displayed 82-fold and 13-fold lower IC50 values than the free Gem, respectively. The UTMD-promoted co-delivery of Gem and miR-21i was further validated by *in vivo* treatment and showed a significant tumor volume reduction and an increase in blood perfusion of xenografted pancreatic tumors.

Conclusion: The co-delivery of Gem and miR-21i using Au DENPs can be significantly promoted by UTMD technology, hence providing a promising strategy for effective pancreatic cancer treatments.

Key words: ultrasound-targeted microbubble destruction; PAMAM dendrimers; gold nanoparticles; drug delivery; gene delivery; pancreatic cancer

Introduction

Pancreatic cancer (PaCa) is one of world's leading causes of cancer mortality and the fourth most common cause of cancer-related death in Europe and the United States [1]. Conventional therapy methods

include curative resection and chemotherapy alone. However, most patients have no chance of surgical resection in the advanced stage with distant metastases and chemotherapy suffers the problems of low drug permeability and inherent or acquired drug resistance [2, 3]. Thus, improved treatment strategies including new chemotherapeutics and drug delivery systems are necessary for enhanced PaCa treatment.

Gemcitabine (Gem; 2', 2'-diflurodeoxycytidine) is the standard chemotherapeutic drug administered to patients with locally unresectable advanced or metastatic PaCa [4]. It is a nucleoside analog that can be incorporated into DNA to create an irreparable error, leading to inhibition of further DNA synthesis and cell death. However, due to inherent chemoresistance of PaCa as well as impaired drug delivery pathways, PaCa patients show modest clinical response to Gem. In addition, Gem shows common side effects like systemic toxicity due to its high dosage and non-specificity with respect to normal cells [5-7]. To overcome these adverse effects, free Gem therapy has been combined with gene therapy as a multi-target chemotherapeutic to treat PaCa [8, 9]. Park *et al*. reported that miRNA-221 inhibitor (miR-221i) and miRNA-21 inhibitor (miR-21i) can be used as a gemcitabine-based combination regimen to produce a synergistic effect in various pancreatic tumor cells [10]. Hence, new and different types of therapies are needed to enhance the anti-proliferative effects of Gem in the treatment of PaCa.

Recently, microRNAs (miRNAs) have received increasing attention in the field of cancer research. miRNAs are a group of small RNAs, which are single-stranded and consist of 18-25 nucleotides (-22 nt). miRNAs function *via* base-pairing with complementary sequences within messenger RNAs (mRNAs) that can inhibit the translation of the mRNAs into protein. miRNAs regulate the proliferation and apoptosis of tumor cells, and their down expression leads to effective tumor inhibition [11-13]. Literature reports show that four types of miRNAs have abnormally high expression in PaCa, including miR-155, miR-21, miR-221 and miR-222, and the miR-21 displays the highest overexpression in PaCa [8, 14]. These results showed that miR-21 was among the top miRNAs with increased expression in PaCa. The mechanism of miR-21 includes modulation of apoptosis, Akt phosphorylation, and expression of genes involved in the invasive behavior in PaCa [15]. Furthermore, miR-21 expression correlated with outcome in PaCa patients treated with Gem. For instance, overexpression of miR-21 leads to downregulation of tumor suppressors phosphatase and tensin homologue (PTEN) and phosphorylation

of its downstream kinase Akt, rendering the cancer cells less susceptible to Gem [10, 16]. Hence, simultaneous delivery of a chemotherapeutic drug and miR-21i has been demonstrated to be an effective strategy for cancer therapy [17, 18]. However, the synthetic naked miRNA inhibitors are unstable in a nuclease rich serum and the development of an effective delivery system capable of co-delivery of Gem and miR-21i still remains challenging.

Dendrimer is a macromolecule characterized by highly branched, abundant surface functional groups, spherical geometry, and monodispersed and well-defined molecular structure. The dendrimer surface and interior can be modified or physically changed for noncytotoxicity, high-efficiency, and specific gene and drug delivery applications [19, 20]. To increase the aqueous solubility and biocompatibility, polyethylene glycol (PEG) can be modified on the dendrimer surface to reduce interactions with serum proteins and shield the positive surface charge [21, 22]. To further improve the gene transfection efficiency, the dendrimers should maintain a 3D conformation to improve their DNA compression capability. For instance, amine-terminated generation 5 (G5) poly(amidoamine) (PAMAM) dendrimers entrapping gold nanoparticles (Au DENPs) are able to well maintain their three-dimensional conformation for enhanced gene delivery applications [23-25]. Further modification of PEG and PEGylated arginine-glycine-aspartic (RGD) peptide onto the surface of Au DENPs enables specific human bone morphogenetic protein-2(hBMP-2) with plasmid DNA(pDNA) delivery to human mesenchymal stem cells [26] and specific siRNA delivery to cancer cells [27]. Although dendrimers have been widely applied in the delivery of anticancer drugs [28-31] or genes [27, 32, 33], there have been few reports related to the co-delivery of genes and drugs using dendrimers as vectors [34], and no reports related to the use of Au DENPs for combinational chemotherapy and gene therapy of PaCa.

PaCa is well known to be a hypovascular tumour with less perfusion than the tissue surrounding it [35, 36]. In order to enhance drug delivery, it is ideal to enlarge the permeability of vessels and the tumor cells. Ultrasound-targeted microbubble destruction (UTMD) is not only an effective approach to monitor the tumor in real-time with high spatial and temporal resolution, but also a useful tool to promote the cellular uptake of drugs or genes by improving the permeability of cancer cells [37-40]. Microbubbles exposed to ultrasound can be destroyed and the resultant cavitation effect is able to enhance cell membrane permeability without deterring the cell viability for desired drug or gene delivery at a specific

tumor site and in a given time period [41-43]. It also has been proven that UTMD can enhance the clathrin-based endocytosis of nanoparticles (NPs) [44]. In our previous study, we have also shown that under a UTMD condition, the delivery of paclitaxol (PTX) by methoxy polyethylene glycol-polylacticco-glycolicacid-polylysine (*m*PEG-PLGA-PLL) NPs can be enhanced for tumor chemotherapy [45, 46].

In this study, we developed a new PEGylated Au DENPs-based delivery system for simultaneous loading and delivery of Gem and miR-21i (Scheme 1). Partially PEGylated G5 PAMAM dendrimers were first used as templates to entrap Au NPs, and the generated Au DENPs were used to sequentially load Gem *via* electrostatic interactions or hydrophobic interactions and miR-21i *via* electrostatic compression. The formed complexes were systematically characterized *via* different methods in terms of structure, size and morphology, drug and gene loading capacity, drug release kinetics, and cytotoxicity. The co-delivery of drug and gene was validated by *in vitro* cell cytotoxicity, apoptosis, western-blot and PCR assays. Finally, the synergistic effects of co-delivery of Gem and miR-21i using UTMD technology were also investigated *in vitro* and *in vivo* using a xenografted tumor model. To our knowledge, this is the first report related to the development of an Au DENP-based delivery system for UTMD-promoted co-delivery of drug and gene for PaCa treatment.

Materials and Methods

Preparation of Au DENPs/miR-21i and Gem-Au DENPs/ miR-21i polyplexes

According to the protocols described in our previous study related to the preparation of PEGylated dendrimers [26] and the formation of Au DENPs [23-25] (see Supplementary Material), we prepared PEGylated Au DENPs for co-delivery of Gem and miR-21i (Scheme S1). The Gem was loaded onto the Au DENPs platform, and the miR-21i (20 µM) was mixed with Gem-Au DENPs solution containing appropriate ratio of primary amines on the vector surface to phosphate groups in the miR-21i backbone (i.e., the N/P ratio). The mixture was gently vortexed and incubated at room temperature for 30 min. The polyplexes were prepared according to the appropriate N/P ratio. The Au DENPs/miR-21i polyplexes without Gem at different N/P ratios were prepared in the same way.
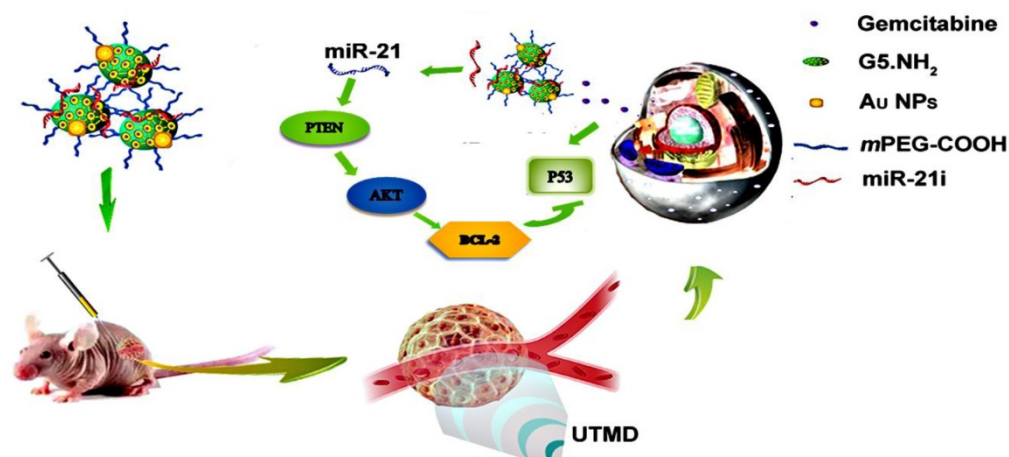
Gel retardation assay

A gel retardation assay was performed to assess the condensation ability of Au DENPs and Gem-Au DENPs. 1% (w/v) agarose gel mixed with 0.1 µg/mL ethidium bromide (EB) was prepared using Tris-acetate-EDTA buffer. Gel electrophoresis was carried out at 80 V for 30 min. The retardation of the Au DENPs/miR-21i and Gem-Au DENPs/miR-21i polyplexes prepared at different N/P ratios was analyzed by a gel image analysis system (Shanghai FURI Science & Technology, Shanghai, China) [27].

Optimization of acoustic cavitation parameters

Acoustic cavitation parameters for sonoporation, in which ultrasound and microbubbles-mediated cavitation generates transient or repairable pores for facilitating cellular uptake of external molecules such as drugs, genes and proteins into living cells—was optimized using fluorescein isothiocyanate (FITC) to study the UTMD-mediated cellular uptake and cell apoptosis under different ultrasound conditions [37].

SW1990 cells were seeded in a 6-well plate at a density of 4.0×10^4 cells per well. After the cells reached 60-70% confluence, the cells were trypsinized and collected in a tube preloaded with FITC in PBS to

Scheme 1. Schematic illustration of Au DENPs-based delivery system for UTMD-promoted co-delivery of drug and gene for PaCa treatment.

have a final concentration of 2 mg/mL for each sample. Then, according to our previous study, SonoVue microbubbles were added into each cell suspension to a concentration of 20% (v/v) [45]. The tube filled with a total of 2 mL mixed suspension was fixed in the tank at room temperature (Fig. S1) and exposed to a 1 MHz therapeutic ultrasound machine (PHYSIOSON-Basic, PHYSIOSON Elektro-medizin, Germany) with 1 kHz pulse repetition frequency (PRF) with a total exposure time of 30 s under different power densities (0.2 W/cm^2, 0.4 W/cm^2 and 0.6 W/cm^2). The half-pressure diameter of the beam was 8.5 mm.

After exposure to ultrasound, samples were placed in the incubator to recover from the effects of cavitation for 30 min, and then were centrifuged at 209 × g for 3 min to remove excess FITC from the extracellular medium. To assess the cell viability after acoustic cavitation treatments, the cells were treated with propidium iodide (PI, 2 μM) that stains the dead cells for 5 min. Then the cells were washed at least twice with PBS and assayed *via* fluorescence activated cell-sorting (FACS, Beckman Coulter, Miami, Florida).

Cytotoxicity evaluation

SW1990 cells were seeded in a 96-well plate at a density of 1.0 × 10^4 cells per well. After 24 h incubation, the cell medium was replaced with 100 μL fresh medium containing 10 μL of Au DENPs or the polyplex solutions at different concentrations in each well. Cells treated with PBS were used as control. For the group of Gem-Au DENPs/miR-21i + U (Gem-Au DENPs/miR-21i combined with UTMD), UTMD was performed using an optimized condition (0.4 W/cm^2, 1 MHz, 20% microbubbles, PRF 1kHz, 30 s). After the cells were cultured for 24 h, 48 h, or 72 h, CCK-8 solution (10 μL) was added to each well, and the cells were incubated for another 4 h at 37 °C before quantification by a Spectra Max 190 microplate reader (BIO-RAD, Hercules, CA) at a wavelength of 450 nm.

Cellular uptake of the polyplexes

To investigate the intracellular localization of the Gem-Au DENPs/ miR-21i polyplexes, confocal laser microscopy (Leica Microsystems, Mannheim, Germany) was applied. SW1990 cells were seeded in 6-well plates at a density of 3.0 × 10^5 cells per well for 24 h to bring the cells to the defined confluence. The medium was replaced with 1 mL fresh medium containing 100 μL Gem-Au DENPs/Cy3-miR-21i polyplexes ([Cy3-miR-21i] = 20 μM, N/P = 8:1) and the cells were incubated for 1 h, 2 h and 4 h. Then the cells were washed three times with PBS, fixed with 5% glutaraldehyde in PBS for 15 min at 4 °C, counter stained with Hoechst 33342 (1 μg/mL) for 30 min at 37 °C to stain the cell nuclei, and further washed three times with PBS. Images of cells were acquired using confocal laser microscopy.

The cellular uptake of Gem-Au DENPs/Cy3-miR-21i polyplexes was also detected by an Accuri C6 Flow cytometer (BD Biosciences, San Diego, CA). The cells were prepared as described above and trypsinized, followed by analysis of the Cy3 fluorescence by flow cytometry.

To study the UTMD-triggered cellular uptake of the polyplexes, cells were seeded in 6-well plates at a density of 3.0 × 10^5 cells per well to reach 70% confluence. Before incubating with Gem-Au DENPs/ Cy3-miR-21i for 4 h, the cell suspension mixed with SonoVue was exposed to the ultrasound apparatus at the optimize parameters (0.4 W/cm^2, 1 MHz, 20% microbubbles, PRF 1 kHz, 30 s). The fluorescence intensity of cells was detected using flow cytometry as described above.

Evaluation of cell apoptosis

SW1990 cells were seeded in 6-well plates at a density of 1.0 × 10^5 cells per well. After 24 h incubation, the cell medium was replaced with fresh medium containing 100 μL of the Au DENPs or the polyplex solutions in each well for another 24 h. Then cells were collected and re-suspended in 100 μL ice-cold binding buffer, followed by addition of 5 μL of Annexin V-FITC and 5 μL of PI solution (BD Biosciences, San Diego, CA). The samples were incubated for 15 min in the dark at room temperature before being subjected to flow cytometry analysis. The assay was performed 3 times for each sample. The cells treated with PBS under the same processes were used as control.

Western blot analysis

SW1990 cells were seeded in a flask at a density of 5.0 × 10^5 cells/mL for 24 h to bring the cells to the defined confluence. The medium was replaced with fresh medium containing Au DENPs or the polyplexes solutions and the cells were incubated for 48 h. The cells were washed with PBS three times and then exposed to 1% cell lysate buffer to extract protein. The whole cell protein lysates were electrophoresed on 10% sodium dodecyl sulfate-polyacrylamide (SDS-PAGE) gels and transferred onto polyvinylidene difluoride membranes (Millipore, Bedford, Massachusetts), followed by blocking in Tris-buffered saline with 5% non-fat milk, and then incubated with primary antibodies at 4°C overnight. The primary antibodies were diluted in PBS as follows: Bcl-2, Bax, P53 and PTEN (Abcam, Cambridge, UK). Membranes were then incubated with secondary antibody (Beyotime, Shanghai, China)

for 1 h at room temperature. The density of target protein signals was visualized using a chemiluminescence imaging system (Tanon, Shanghai, China).

In vivo antitumor activity study

All animal studies were approved by the Shanghai Jiaotong University Animal Care and Use Committee and performed in accordance with guidelines and regulations of National Ministry of Health. A total of 36 female athymic BALB/c nude mice (4-6 weeks old) weighing 18-20 g were purchased from Sippr-BK laboratory animal Co. Ltd (Shanghai, China) and kept in the Laboratory Animal Center of Shanghai General Hospital (Shanghai, China). These mice were maintained in a pathogen-free environment (23 ± 2 ℃ and 55% ± 5% humidity).

In order to establish a xenografted mouse tumor model, 1×10^6 SW1990 cells were collected and subcutaneously injected into the back of the BALB/c nude mice. When the tumor volume reached 32-80 mm³ at 14 days, the mice were divided into four groups (n = 9 for each group): Control (PBS, 100 μL), free Gem (10 mg/kg, in 100 μL PBS), Gem-Au DENPs/miR-21i ([Gem] = 10 mg/kg, [miR-21i] = 20 μM, in 100 μL PBS), and Gem-Au DENP/miR-21i + U ([Gem] = 10 mg/kg, [miR-21i] = 20 μM, in 100 μL PBS). Each tumor-bearing mouse was intratumorally injected with the polyplexes every other day for 3 weeks. For the Gem-Au DENPs/miR-21i + U group, the US transducer (PHYSIOSON-Basic, PHYSIOSON Elektro-medizin, Germany) was positioned above the tumor, and SonoVue (1.18 mg/mL, in 0.2 mL saline) was slowly injected via tail vein after intratumoral injection of Gem-Au DENPs/miR-21i polyplexes. According to a previous study, the tumors were insonated percutaneously for 2 min to achieve the longest active sonoporation time (1 MHz, 0.4 W/cm², 20% microbubbles) [45, 46].

Every three days, the growth of tumors in nude mice was observed by ultrasound imaging using B-mode to evaluate the tumor size by a clinical diagnosis ultrasound scanner (LOGIQ E9, GE, Fairfield, Connecticut). The tumor volume was calculated by the equation: $V = L \times W^2/2$, where V is the tumor volume, L is the tumor length and W is the tumor width. The largest cross-section and longitudinal-section of each tumor was taken to ensure the same condition. Body weight was also recorded every three days. At the end of the treatment course, contrast-enhanced ultrasound (CEUS) was performed to record the perfusion process and capture the morphological changes of tumors for 2 min. In this study, 3 mice were randomly selected from each group to undergo CEUS after injection of SonoVue (1.18 mg/mL, in 0.1 mL saline for each mouse) through orbital vein, and the same probe (LOGIQ E9, ML 6-15 MHz) was used for the contrast modality at a low mechanical index (0.12). All CEUS images were performed in the same condition of 20 mm depth and 10 gains. To investigate the perfusion process, the perfusion curve of a region of interest (ROI) was generated after injection of SonoVue, and the perfusion index within the ROI was calculated by CEUS immediately at the end of treatment. The perfusion index corresponds to blood flow within an ROI and is the ratio of the area under the curve (AUC) to mean transit time (MTT). The MTT is the contrast agent circulation time in the ROI of the tissue.

After CEUS, the mice were anesthetized and dissected to analyze the tumor pathological changes and toxicity by hematoxylin and eosin (H&E) and TUNEL staining according to standard protocols [46]. The remaining animals were used to observe the survival rate (n = 6).

Statistical analysis

All data are represented by mean ± standard deviation. Statistical analysis was performed using variance tests (two-way ANOVA and one-way ANOVA). Data sets were compared using two tailed, unpaired t-test. A value of 0.05 was set as the significance level; the data were marked as (*) $p < 0.05$, (**) $p < 0.01$, and (***) $p < 0.001$.

Results and discussion

Characterization of Au DENPs polyplexes

In this study, G5 PAMAM dendrimers were selected for the synthesis of a multifunctional drug and gene delivery vector due to their relative stability, large internal cavities and numerous terminal amine groups that can be modified with different functionalities [47-50]. To better improve the gene transfection efficiency, Au DENPs were synthesized using G5.NH₂-*m*PEG dendrimers as templates and characterized using UV-vis spectroscopy and TEM. Fig. 1A shows the UV-vis spectrum of Au DENPs, where an absorption peak at about 510 nm can be assigned to the typical surface plasmon band of Au NPs, indicating the successful formation of Au DENPs. ICP-OES was used to analyze the loading of Au NPs within the G5.NH₂-*m*PEG dendrimers. We show that there were about 25 equiv. (i.e., 25 Mole) of Au loaded within each G5.NH₂-*m*PEG dendrimer. TEM was used to characterize the morphology and size distribution of the Au core particles in the Au DENPs. All Au core NPs exhibited a spherical shape and were distributed evenly with an average size of 2.6 nm (Fig. 1B, C).
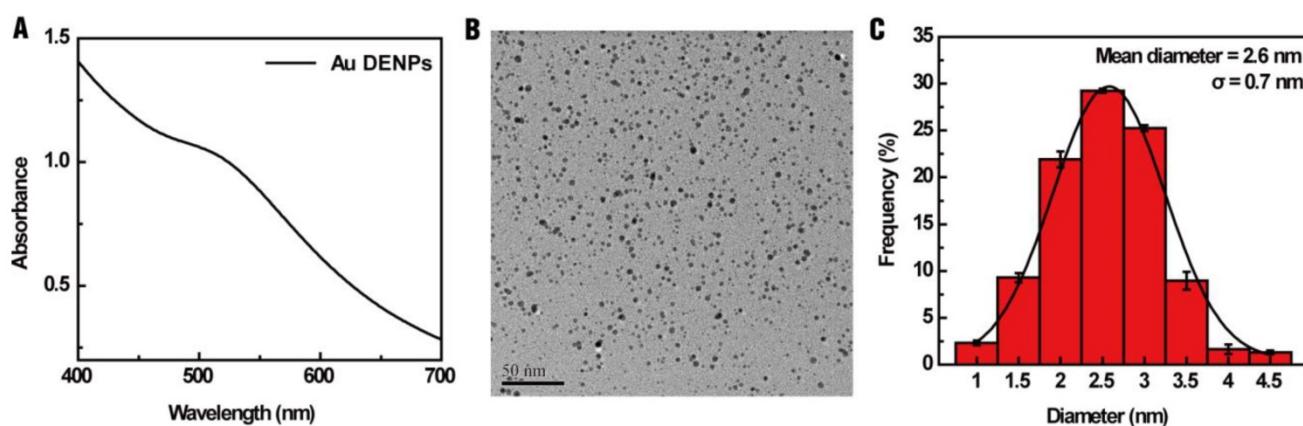
Figure 1. (**A**) UV-vis spectrum, (**B**) TEM image, and (**C**) size distribution histogram of the Au DENPs

Characterization of the designed vector/miR-21i polyplexes

To evaluate the RNA compression ability of Au DENPs, a gel retardation assay was performed. As shown in Fig. 2A, the mobility of miR-21i was able to be retarded at a N/P ratio of 2:1 or greater. To investigate if the encapsulation of Gem within Au DENPs impacts the RNA compaction ability of the vector, the miR-21i retardation of Gem-Au DENPs was also evaluated. Fig. 2B shows that the migration of miR-21i can also be retarded at a N/P ratio of 2:1 or above, confirming that the loading of Gem does not impact the compaction capability of the Au DENPs.
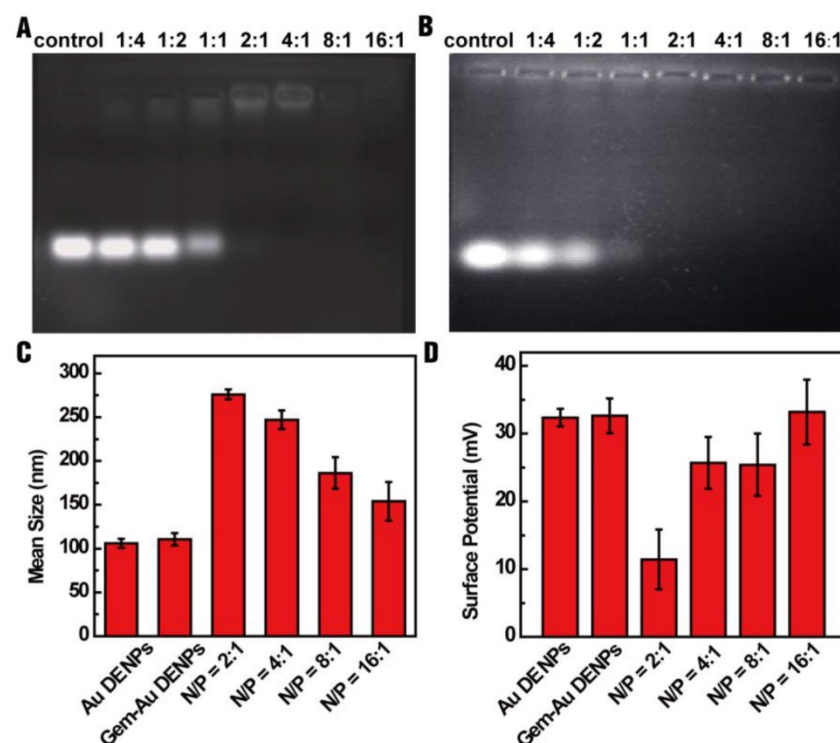
For gene transfection studies, the designed vector/miR-21i polyplexes should have an appropriate size and relative positive surface potential. Therefore, dynamic light scattering (DLS) and zeta potential measurements were applied to characterize the polyplexes. The results reveal that the mean hydrodynamic size of the polyplexes (in a range of 154-276 nm) decreases with an increase in the N/P ratio (Fig. 2C) and the surface potential of the polyplexes increases as the N/P ratio increases (Fig. 2D). The surface potential of the polyplexes has a range of 11-33 mV; this result is in line with our previous studies [25, 27] and suggests the formed Gem-Au DENPs/miR-21i polyplexes may be considered as suitable transfection materials at a N/P ratio of 2:1 or above. It should be noted that between the N/P ratios of 4:1 and 8:1, the surface potential did not significantly change. Since only the Au DENPs covering the surface of the polyplexes contribute to the surface potential of the polyplexes, this suggests that the interaction between Au DENPs and miR-21i at a N/P ratio of 8:1 reached saturation and has the most suitable surface potential for gene delivery. Therefore, we selected the Gem-Au DENPs/miR-21i at a N/P ratio of 8:1 for further studies.

Identification of ultrasound exposure parameters for cellular uptake of polyplexes

Studies had shown that fluorescent molecules (e.g., FITC) can directly penetrate into the cytosol through the pores caused by UTMD, which can be used to study the

Figure 2. Gel retardation assay (**A**) of Au DENPs/miR-21i and (**B**) Gem-Au DENPs/miR-21i at different N/P ratios. Mean hydrodynamic size (**C**) and surface potential (**D**) of Au DENPs, Gem-Au DENPs, and Gem-Au DENPs/miR-21i under different N/P ratios (mean ± SD, n = 3).

cellular uptake efficiency [37, 51]. To examine the optimum parameters for ultrasound-enhanced cellular uptake of NPs, a platform suitable for ultrasound exposure *in vitro* was established (Fig. S1). Fig. 3 shows the dot-plots of cells stained with FITC and PI, and the quantitative analysis of the FITC uptake efficiency and cell viability with different treatments. The FITC uptake efficiency can be used to reflect the number of sonoporated cells. Clearly, control cells exhibited minimal FITC uptake efficiency (1.61% ± 0.36%) and high cell viability (98.49% ± 0.36%). In contrast, the cells after treatment with ultrasound power densities of 0.4 W/cm², and 0.6 W/cm² displayed high FITC uptake efficiencies of 15.72% ± 1.16%, and 16.94% ± 1.13% compared to control cells, suggesting that the cells could be sonoporated after treatment with ultrasound exposure. Moreover, the total numbers of sonoporated cells in the 0.4 W/cm² and 0.6 W/cm² groups were significantly greater than those in the 0.2 W/cm² group and control group ($p < 0.001$). However, no significant difference between the 0.2 W/cm² group (2.10% ± 0.62%) and the control group could be observed ($p > 0.05$). This could be because the power density of 0.2 W/cm² mainly results in stable cavitation, in which microbubbles stably oscillate without collapsing in an acoustic field, resulting in weak sonoporation effects, in agreement with the literature [52, 53]. Although the FITC uptake efficiency in the 0.6 W/cm² group was greater than that in the 0.4 W/cm² group, there was no statistical significance between the two groups. Additionally, the cell viability in the 0.6 W/cm² group was lower than that in the 0.4 W/cm² group ($p < 0.01$). Considering all the above results, we therefore selected 0.4 W/cm² as the optimum power density for the follow-up experiments.

Therapeutic efficacy of Gem-Au DENPs/miR-21i polyplexes

The therapeutic efficacy of Gem for pancreatic cancer cells was reported to be dose- and time-dependent and the peak cytoplasma concentration of Gem was reported to be 100 µM [17]. In this study, the cytotoxicity of the Au DENPs or the polyplexes was assessed by the CCK-8 cell viability assay (Fig. 4 and Fig. S5). As shown in Fig. S5, the SW1900 cells treated with the Au DENPs displayed the same viability as those treated with PBS, indicating that the Au DENPs are non-toxic in the studied concentration range. The cell viability of cells treated with Au DENPs/miR-21i still remained at a high level (> 70%) even after 72 h treatment in the studied concentration range, suggesting the weak cytotoxicity of the single-mode gene therapy. For cells treated with different formulations of Gem, the cell viability gradually decreased with increasing Gem concentration and treatment time (Fig. 4A-C). The cell viability of the free Gem group was much lower than that of the Gem-Au DENPs group after 24 h treatment. However, the two groups displayed similar cell viability at 48 h and a slight decrease in the Gem-Au DENPs group at the 72 h time point. This could be due to the fact that the free Gem could passively diffuse into the cell nucleus more quickly than the Gem-Au DENPs during a short time period, while Gem-Au DENPs is able to gradually release Gem in the cytoplasm and therefore the cytotoxicity is cumulative over time *in vitro*. Additionally, both of the two co-delivery groups with and without UTMD treatment (Gem-Au DENPs/miR-21i and Gem-Au DENPs/miR-21i + U) displayed obvious reduction of viability compared to the single-mode therapy, suggesting that miR-21i can act as a cytostatic agent to adjuvant chemotherapy and increase the drug sensitivity [54, 55]. Moreover, the co-delivery group of Gem-Au DENPs/miR-21i + U exhibited less cell viability than the group of Gem-Au DENPs/miR-21i, further demonstrating the additional role UTMD plays to improve the anti-proliferative effect.

The therapeutic effects of different formulations of Gem were further confirmed by measuring their half maximal inhibitory concentrations (IC50) at 24 h, 48 h and 72 h, respectively (Fig. 4D). Free Gem had an IC50 of 1.55 ± 0.26 µg/mL, 0.68 ± 0.09 µg/mL and 0.66 ± 0.07 µg/mL at 24 h, 48 h and 72 h, respectively. Gem-Au DENPs/miR-21i displayed an IC50 of 0.48 ± 0.14 µg/mL, 0.18 ± 0.06 µg/mL, and 0.05 ± 0.01 µg/mL after 24 h, 48 h and 72 h treatment, respectively, showing a time-dependent effect. At each time point, the IC50 of Gem-Au DENPs/miR-21i was significantly lower than that of free Gem ($p < 0.01$). However, this was not the case for Gem-Au DENPs, which only had a lower IC50 value than free Gem at 72 h. Furthermore, compared to Gem-Au DENPs/miR-21i, Gem-Au DENPs/miR-21i + U exhibited relatively low IC50 values at the same time points, which were 0.096 ± 0.008 µg/mL, 0.023 ± 0.016 µg/mL, and 0.008 ± 0.002 µg/mL at 24 h, 48 h and 72 h, respectively. Specifically, Gem-Au DENPs/miR-21i and Gem-Au DENPs/miR-21i + U displayed 13-fold and 82-fold lower IC50 values than free Gem at 72 h, respectively. Taken together, the co-delivery of Gem and miR-21i after UTMD treatment could significantly improve the therapeutic efficacy due to the enhanced cell permeability and the combination chemotherapy and gene therapy.
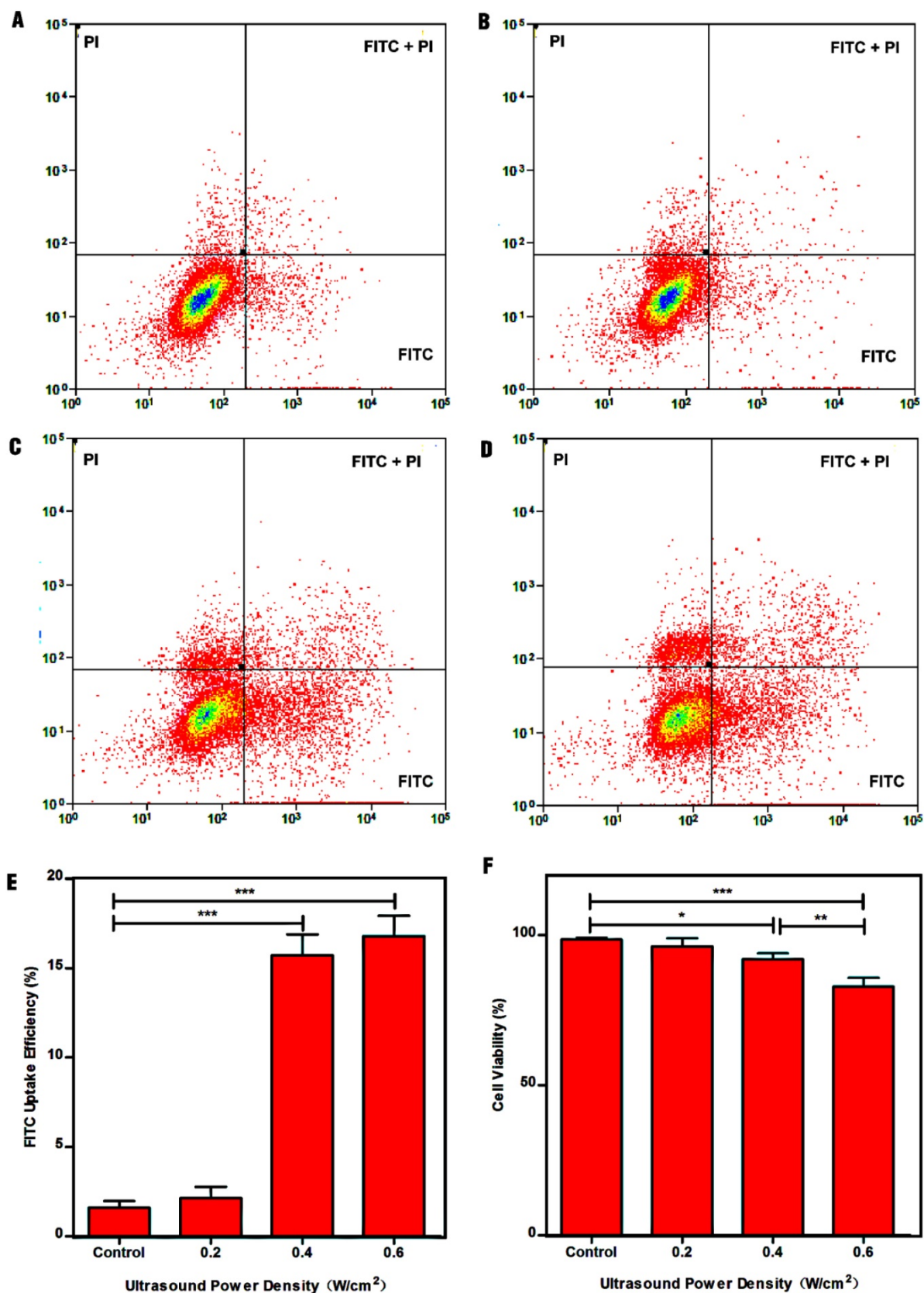
Figure 3. Impact of ultrasound power density on cell permeability and cell apoptosis. (**A**) Control cells without treatment, (**B**) 0.2 W/cm², (**C**) 0.4 W/cm², and (**D**) 0.6 W/cm². (**E**) Efficiency of FITC uptake by cells as a function of ultrasound power density. (**F**) Cell viability after treatment with ultrasound powers of different densities.
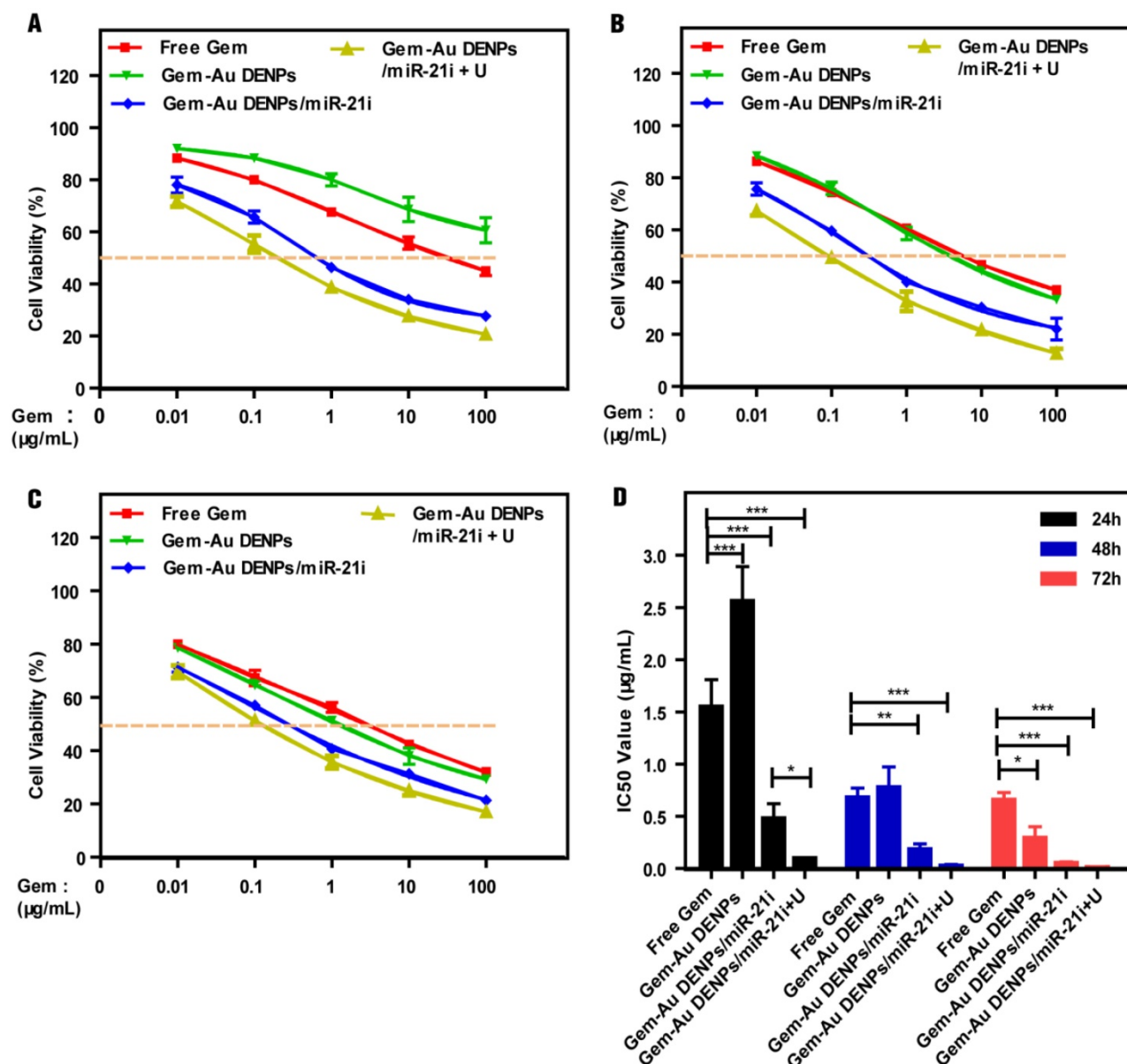
Figure 4. Concentration-dependent cytotoxicity of SW1990 cells treated with free Gem, Gem-Au DENPs, Gem-Au DENPs/miR-21i and Gem-Au DENPs/miR-21i + U evaluated by CCK-8 assay at (**A**) 24 h, (**B**) 48 h, and (**C**) 72 h. (**D**) IC50 values of free Gem, Gem-Au DENPs, Gem-Au DENPs/miR-21i and Gem-Au DENPs/miR-21i + U groups.

Intracellular uptake assay of Gem-Au DENPs/miR-21i polyplexes in SW1990 cells

The cellular uptake of Gem-Au DENPs/miR-21i polyplexes was investigated using confocal microscopy and flow cytometry at different time points. Cy3-labeled miR-21i was used to track the intracellular delivery of Gem-Au DENPs/Cy3-miR-21i polyplexes in SW1990 cells. Fig. 5 shows the confocal microscopy images of cells treated with Gem-Au DENPs/Cy3-miR-21i polyplexes for different time periods. At 1 h treatment, obvious Cy3 fluorescence signals on the surfaces of the cells and also partly in the cytoplasm can be seen, suggesting that the polyplexes could be quickly uptake by the cells. At the time points of 2 h and 4 h, more red fluorescent dots were observed in the cytoplasm, indicating the cellular internalization of the polyplexes (Fig. 5). Similarly, the fluorescence intensity of Gem-Au DENPs/Cy3-miR-21i complexes was analyzed by flow cytometry and the results were in accordance with the confocal microscopy observations (Fig. S6).

Studies have demonstrated that UTMD can enhance the permeability of the cell membrane and increase the delivery of nanoparticles to cells by the effects of sonoporation [42-46], and the therapeutic effects evoked through sonoporation have been observed for several days with prolonged therapeutic

results. At the same, our previous studies reported that UTMD increased the expression and accumulation of clathrin over a few hours, thus enhancing clathrin-mediated endocytosis [44-46]. In order to further confirm the UTMD-enhanced polyplexes delivery, the cells were incubated with Gem-Au DENPs/Cy3-miR-21i polyplexes for 4 h and exposed to an ultrasound exposure condition. The confocal microscopy images (Fig. 5) and flow cytometry analysis (Fig. S6) show that the cells treated with the polyplexes for 4 h had higher fluorescence intensity in the cytoplasm than those without treatment of UTMD at the same conditions. The increased uptake of polyplexes is probably a consequence of UTMD causing an increase in the number of pores and clathrin. These data suggest that UTMD can promote the delivery of Gem-Au DENPs/Cy3-miR-21i polyplexes at a cellular level.

Cell apoptosis assay

To further investigate the cell apoptosis efficiency, SW1990 cells treated with the Au DENPs or the polyplexes for 24 h were analyzed by flow cytometry (Fig. 6). No obvious cell apoptosis of the Au DENPs group (Fig. 6B) could be seen when compared to the control group (Fig. 6A). However, cells treated with the Au DENPs/miR-21i (Fig. 6C) had an apoptosis percentage of 4.03% ± 0.84%, which was significantly higher than the control group (1.33% ± 0.15%, $p < 0.01$), suggesting the gene inhibition effect of the miR-21i (Fig. 6H). Additionally, all of the other four groups containing Gem (Fig. 6D-G) exhibited obvious cell apoptosis trends compared to the control group ($p < 0.001$). As expected, the cell apoptosis percentage of the Gem-Au DENPs/miR-21i group (20.87% ± 0.81%) and Gem-Au DENPs/miR-21i + U group (25.43% ± 0.60%) were much higher than that of the free Gem group (10.50% ± 0.56%). Moreover, there was a significant difference in the cell apoptosis percentage between the Gem-Au DENPs/miR2-1i group and the Gem-Au DENPs/miR-21i + U group (p < 0.001). These results indicate that the co-delivery system could achieve the synergistic gene/chemotherapeutic efficacy, and the UTMD treatment could further enhance the synergistic efficacy.

To investigate the apoptosis pathway, SW1990 cells were incubated with different forms of the Au DENPs or the polyplexes for 24 h, the expressions of the apoptosis-related proteins including Bax and P53 (playing a critical role in the mitochondrial apoptotic pathway), and Bcl-2 (the anti-apoptotic proteins as downstream targets of miR-21) and PTEN (tumor suppressor [56]) were tested by western blot assays. The four relative protein
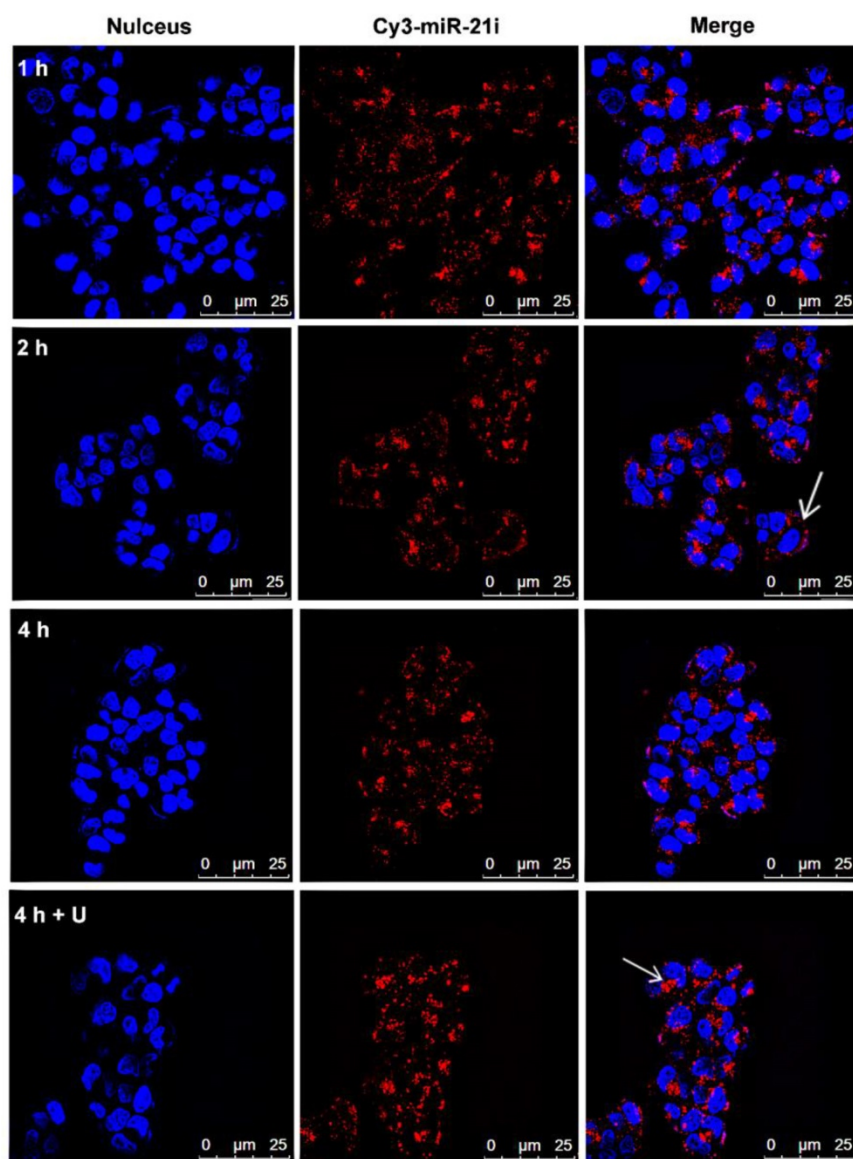
Figure 5. Confocal microscopy images of SW1990 cells co-cultivated with Gem-Au DENPs/Cy3-miR-21i polyplexes for different time periods (red, Cy3-miR-21i; blue, Hoechst 33342, nuclear staining). White arrow head points to Gem-Au DENPs/Cy3-miR-21i polyplexes observed in the cytoplasm.

expressions of cells treated with Au DENPs had no significant differences compared to that of the control group, suggesting the cytocompatibility of Au DENPs under a certain studied concentration (Fig. S7). As shown in Fig. 7, after treatment with Au DENPs/miR-21i, free Gem, or Gem-Au DENPs, the relative protein expressions started to exhibit a lower level of Bcl-2, and a higher level of PTEN, Bax and P53 than the control group, which demonstrates activation of the apoptosis pathway due to the presence of miR-21i or Gem. Additionally, both of the two co-delivery groups displayed dramatically increased PTEN, Bax and P53 and obvious reduction of Bcl-2 compared to the other groups. Moreover, the greatest reduction of Bcl-2 and the fastest increase of PTEN were shown in the Gem-Au DENPs/miR-21i + U group, indicating that the combined therapy achieved a significant killing efficacy by the inhibition of downstream targets of miR-21. The PCR results (Fig. S7) for the apoptotic pathway evaluation are consistent with the data of the western blot assay. Taken together, these results demonstrate that the Au DENPs loaded with Gem and miR-21i can activate the mitochondrial apoptosis pathway and miR-21-mediated apoptosis pathway, achieving an enhanced efficacy in treating the SW1990 cells. Furthermore, UTMD plays a significant role in the promotion of the apoptosis pathways.
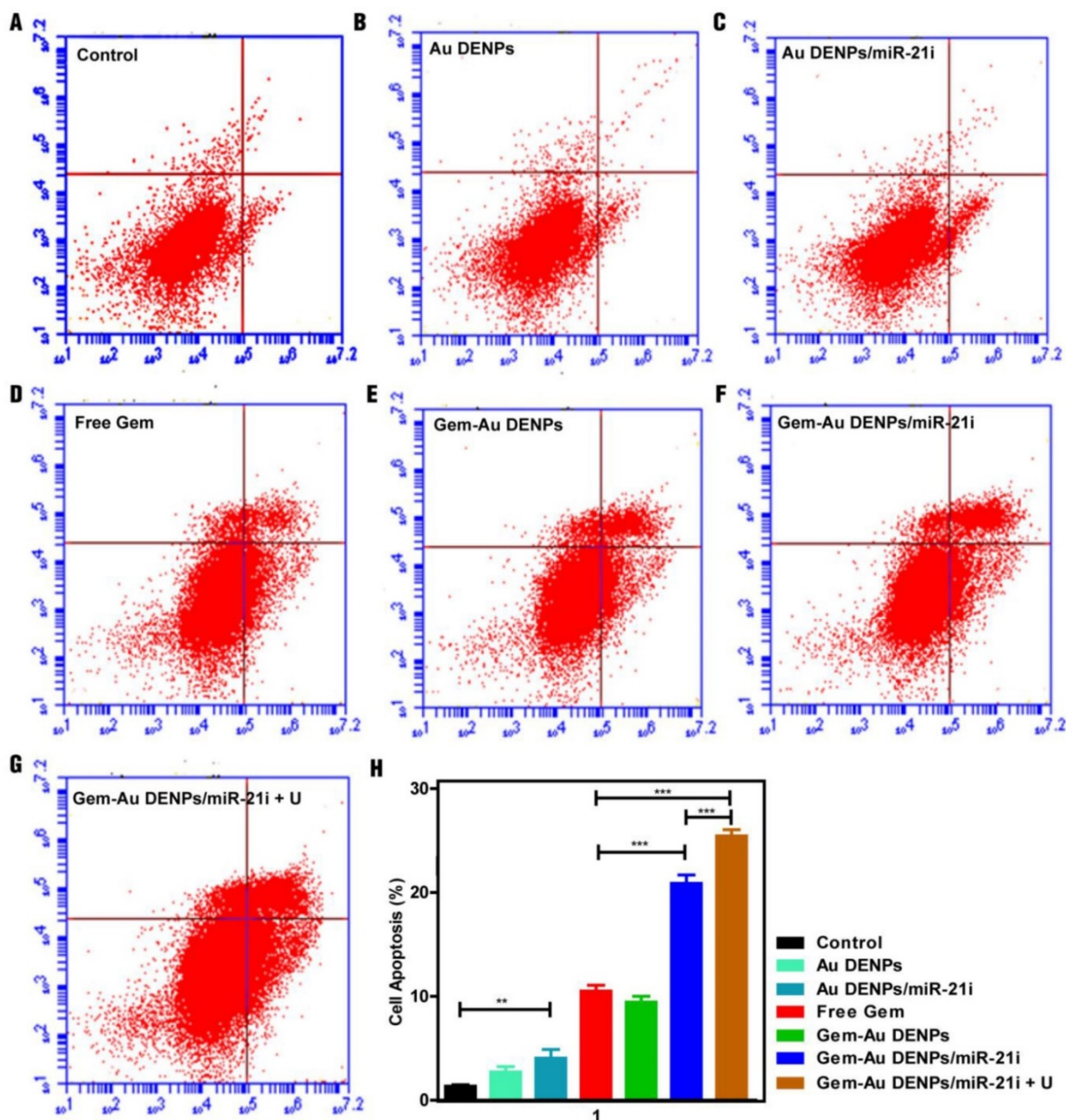

Figure 6. Apoptosis assay of cells under different treatments after double staining with Annexin V- FITC/PI and measurement by flow cytometry. (**A**) Control group, (**B**) Au DENPs group, (**C**) Au DENPs/miR-21i group, (**D**) free Gem group, (**E**) Gem-Au DENPs group, (**F**) Gem-Au DENPs/miR-21i group, and (**G**) Gem-Au DENPs/miR-21i + U group. (H) Apoptosis percentage of cells with different treatments. Data are shown as mean ± SD (n=3).
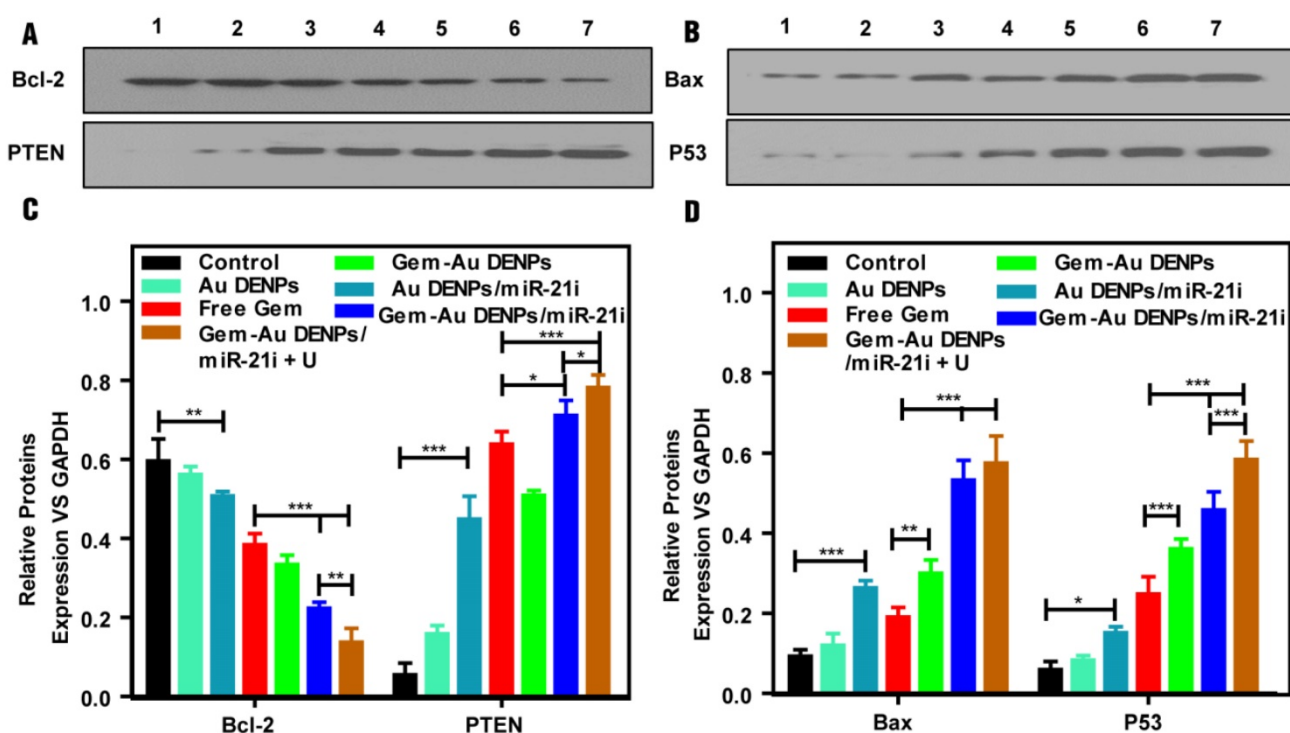
Figure 7. (**A, B**) Apoptotic pathway analysis of SW1990 cells treated with the Au DENPs or the polyplexes *in vitro* under different treatment conditions. Lane 1: Control, lane 2: Au DENPs, lane 3: Au DENPs/miR-21i, lane 4: free Gem, lane 5: Gem-Au DENPs, lane 6: Gem-Au DENPs/miR-21i, lane 7: Gem-Au DENPs/miR-21i + U. (**C, D**) Quantitative analysis of protein expression based on Western blotting assay.

In vivo therapeutic effect study

A xenografted SW1990 tumor model in mice was established to study the therapeutic efficacy of different forms of Gem *in vivo*. Firstly, B-mode ultrasound imaging was used to monitor the tumor size after different treatments. As shown in the tumor ultrasound images after different treatments for 21 days (Fig. 8A), we can visually observe that the tumor size after treatment in the co-delivery groups was smaller than that of the free Gem and control groups. The tumor volume changes after different time points were also recorded and analyzed to evaluate the therapeutic effect. As shown in Fig. 8C, the tumor volumes of mice treated in the co-delivery groups were also much smaller than those of the free Gem and control groups ($p < 0.001$), suggesting the enhanced combinational therapeutic effect. Furthermore, the Gem-Au DENPs/miR-21i + U group displayed a significant tumor volume reduction compared to the Gem-Au DENPs/miR-21i group without UTMD treatment ($p < 0.001$), indicating the enhanced role of UTMD during the antitumor process.

In addition, the subcutaneous pancreatic tumor vascularity after treatment was also observed by means of CEUS imaging to assess the therapeutic effect. CEUS imaging is a promising, reliable modality that can reveal tumor vascular flow and could be potentially useful to evaluate treatment effect after chemoradiotherapy [35, 36, 57]. CEUS images (Fig. 8B) show the tumor vascularity and intratumoral blood perfusion changes after treatment for the different groups. More abundant intratumoral blood perfusion was detected in the co-delivery groups, indicating their better prognosis [37-40]. A potential consequence of the increase in blood perfusion in the Gem-Au DENPs/miR-21i group is an increase in the enhanced permeability and retention effect (EPR effect), in which NPs efficiently accumulate and release drugs at the tumor site for a longer time period resulting in much more cellular uptake in the tumor tissue [58]. The quantitative analysis of the perfusion index further verifies the above results (Fig. 8D). The tumors treated in the co-delivery groups showed much more blood perfusion than those treated with free Gem and the control group ($p < 0.001$). Moreover, the perfusion index of the Gem-Au DENPs/miR-21i + U group was significantly higher than that of the Gem-Au DENPs/miR-21i group without UTMD treatment ($p < 0.05$). This could be due to the fact that the microbubbles flow through the vasculature allowing direct contact with endothelial cells and increase the vascular permeability by the effect of sonoporation, resulting in enhanced blood flow and hence more drug or gene uptake for efficient treatment [59-61]. These data demonstrate that the co-delivery system and the application of UTMD

could significantly enhance the tumor inhibition effect and improve the intratumoral blood perfusion, which is consistent with our previous study [46, 62].

The tumor apoptosis *in vivo* was also analyzed by TUNEL staining. Since the broken DNA strand of apoptotic tumor cells can be labeled with fluorescence indicators at the exposed free 3'-OH termini in an enzymatic reaction by terminal deoxynucleotidyltransferase (TdT), the TUNEL-positive cell nuclei after different treatments can be detected and quantified by fluorescence microscopy. As shown in Fig. 9A, the highest fluorescence intensity was observed in the Gem-Au DENPs/miR-21i + U group. The TUNEL-

positive cells of the Gem-Au DENPs/miR-21i (53.83% ± 5.28%) and Gem-Au DENPs/miR-21i + U (76.33% ± 3.85%) groups were significantly higher than that of the control (2.93% ± 1.36%) and free Gem (22.55 ± 2.99%) groups ($p < 0.001$) (Fig. 9C), and there was also a statistically significant difference between the Gem-Au DENPs/miR-21i and Gem-Au DENPs/miR-21i + U groups ($p < 0.001$). Similarly, H&E staining (Fig. 9B) shows that tumors treated with Gem-Au DENPs/miR-21i + U exhibit remarkable nucleus atypia and increased necrotic cells, indicating the best therapeutic effect resulted from the enhanced therapy in PaCa.
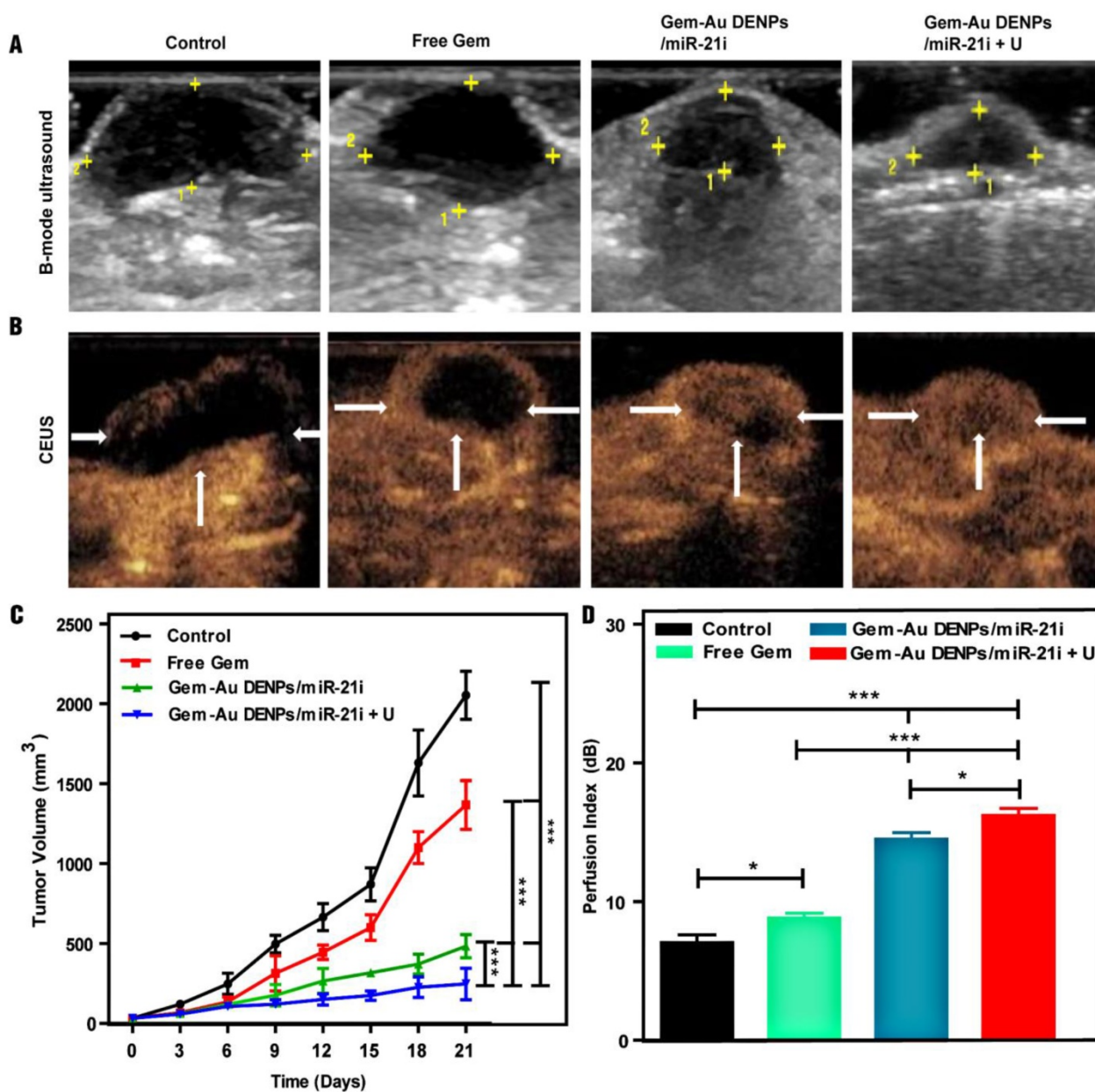

Figure 8. Ultrasound images and therapeutic effect evaluation of tumors *in vivo*. (**A**) B-mode ultrasound image; the yellow dots indicate the region of tumor. (**B**) Contrast-enhanced ultrasound (CEUS) image. CEUS imaging shows abundant intratumoral blood flow with smaller tumor volume in the Gem-Au DENPs/miR-21i + U group. (**C**) Graphs of tumor volume change after different treatments *in vivo*; day 0 is the first day of treatment. (**D**) The perfusion index of mice bearing tumors in the control, free Gem, Gem-Au DENPs/miR-21i and Gem-Au DENPs/miR-21i + U groups after treatment. Data are shown as the mean ± SD (n=3).
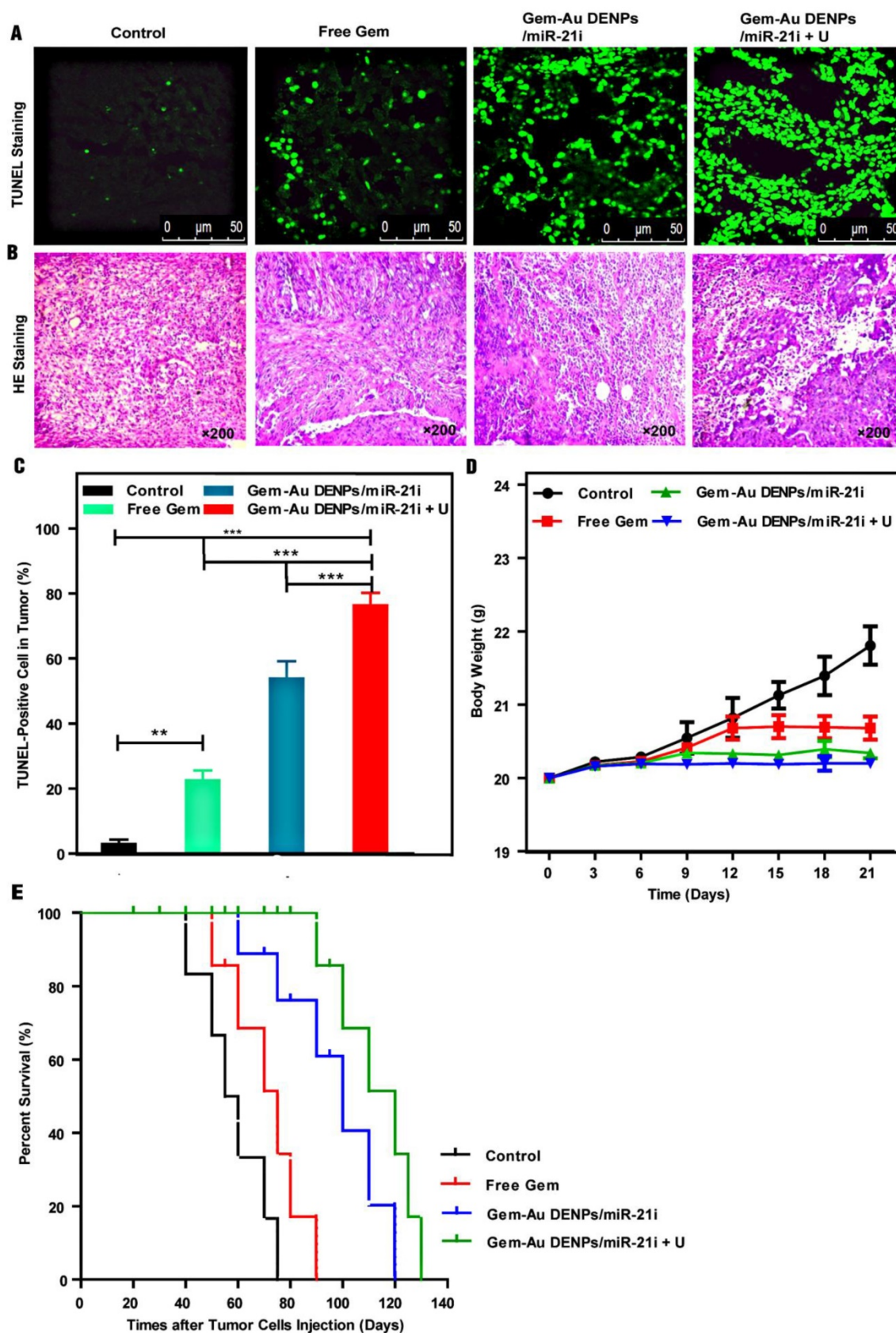
Figure 9. Tumor immunohistochemistry and survival evaluation after treatment. (**A**) TUNEL staining of tumors cells treated with different groups; the green spots represent the TUNEL-positive cells detected in each group. (**B**) H&E staining of tumor cells. (**C**) Quantitative analysis of cell apoptosis percentages from the TUNEL-stained images; the positive cells were quantified by Image Pro Plus Software and counted from four different fields-of-view. (**D**) The mouse body weight change after different treatments; day 0 is the first day of treatment. (**E**) Survival rate of tumor-bearing mice in different treatment groups. Log-rank test showed that the survivals of the Gem-Au DENPs/miR-21i and Gem-Au DENPs/miR-21i + U groups were significantly different from the control group ($p = 0.0088$ and $p = 0.0002$, respectively).

We also evaluated the systemic toxicity of the co-delivery systems by monitoring the body weights of mice for 21 days (Fig. 9D). The control and free Gem groups displayed increasing body weight with time, which may be due to the increasing tumor volumes of the two groups. However, the treatment of the co-delivery systems with or without UTMD did not seem to significantly change the body weights of the mice, suggesting that the co-delivery systems do not have obvious toxic side effects to the mice. Additionally, the biodistribution of Gem-Au DENPs/Cy3-miR-21i (Fig. S8) and their pharmacokinetics (Fig. S9) reveal that the accumulation of Gem-Au DENPs/miR-21i in tumors was significantly increased by their good biocompatibility *in vivo* and further enhanced by UTMD in mouse pancreatic tumor xenografts.

Finally, the therapeutic efficacy of different groups was quantified by calculating the survival rate of mice (Fig. 9E). The median survival rate as analysed by a Kaplan-Meier test followed the order of Gem-Au DENPs/miR-21i + U (120 days) > Gem-Au DENPs/miR-21i (100 days) > free Gem (75 days) > control (57.5 days). The mice treated with the co-delivery groups exhibited much longer survival times than those of the free Gem and control groups. Meanwhile, the survival rate of the Gem-Au DENPs/miR-21i + U group was much higher than that of the Gem-Au DENPs/miR-21i without UTMD application group at the same treatment time, further indicating that UTMD plays a significant role in promoting PaCa treatment. These results revealed that the therapeutic effect of the combination therapy is superior to free Gem treatment, and the employment of UTMD could further prolong the survival rate of mice bearing pancreatic cancer.

Conclusions

In summary, we have developed a UTMD-promoted efficient nanoplatform based on Au DENPs for co-delivery of Gem and miR-21i into cancer cells. Our results show that the Au DENPs are able to encapsulate 30 Gem per dendrimer and compress miR-21i at a N/P ratio of 2:1 or above, and the formed complexes possess a positive surface potential (11-33 mV) and hydrodynamic size of 154-276 nm. Under the promotion of UTMD, the co-delivery of Gem and miR-21i using the Au DENPs can be much more enhanced, as confirmed by the enhanced cellular uptake of the polyplexes, the enhanced therapeutic efficacy *in vitro*, the enhanced cell apoptosis rate *in vitro* along with the apoptosis pathway analysis from a molecular biology perspective, and the enhanced tumor inhibition efficacy *in vivo.* Taken together, our data suggest that UTMD-promoted co-delivery of Gem and miR-21i using Au DENPs may be used as a promising technology for enhanced therapy of PaCa. However, there are limitations to this study.

The primary limitation of this study is that the treatment effect was mainly evaluated using intratumoral injection. While this method gives an enhanced inhibition of tumor progression, and the pharmacokinetics and biodistribution studies by intravenous injection were added to evaluate the metabolism and accumulation of Gem-Au DENPs/miR-21i *in vivo*, it does not take into account the clinical setting. Future work should evaluate the treatment effect in an orthotropic tumor model by intravenous injection, not only by intratumoral injection.

In the field of sonoporation, it is typically assumed to imitate the *in vivo* environment to study the enhanced effect of drug or genes delivery. In our work, the acoustic apparatus is a static model without flow through the ultrasound beam and the range of acoustic parameters for optimal delivery was limited to this ultrasound system. Therefore, much more work should aim to improve the acoustic apparatus to induce the highest therapeutic effect.

Abbreviations

PaCa: Pancreatic Cancer; PAMAM: Poly amidoamine; Au NPs: gold nanoparticles; Au DENPs: Dendrimers-entrapped gold nanoparticles; Gem: Gemcitabine; PEG: Poly(ethylene glycol); UTMD: Ultrasound-targeted microbubble destruction; DEPC: Diethylpyrocarbonate; FITC: Fluorescein isothiocyanate; PRF: Pulse repetition frequency; PVDF: Polyvinylidene fluoride; CEUS: Contrast-enhanced ultrasound; TEM: Transverse electric and magnetic field; AUC: Area under the curve; MTT: Mean transit time; IC50: Half maximal inhibitory concentration; TUNEL: Terminal deoxynucleotidyl transferase-mediated deoxyuridine triphosphate nick-end labeling; TdT: Terminal deoxynucleotidyltransferase; EPR effect: Enhanced permeability and retention effect.

Acknowledgements

Agência Regional para o Desenvolvimento da Investigação Tecnologia e Inovação through the project M1420-01-0145-FEDER-000005-Centro de Química da Madeira-CQM + (Madeira 14-20).

Supplementary Material

1. Ultrasound exposure equipment, see the Figure S1.

2. Synthesis and characterization of G5.NH$_2$-*m*PEG, see the Figure S2.

3. Preparation of Gem-Au DENPs polyplexes and *in vitro* release assay, see the Figure S3-4 and Table S1.

4. Cytotoxicity assay of Au DENPs and Au DENPs/miR-2li, see the Figure S5.

5. Cellular uptake assays of Gem-Au DENPs/miR-21i by flow cytometry, see the Figure S6.

6. Cell apoptosis response by PCR analysis, see the Figure S7.

7. Dynamic fluorescence biodistribution of Gem-Au DENPs/miR-21i polyplexes in mouse pancreatic tumor xenografts by intravenous injection, see the Figure S8.

8. *In vivo* pharmacokinetic evaluation of Gem-Au DENPs/miR-21i polyplexes by intravenous injection, see the Figure S9 and Table S2.

9. *In vivo* therapeutic evaluation of Gem-Au DENPs/miR-21i polyplexes *by* intravenous injection, see the Figure S10.

10. *In vivo* histological analysis of mouse organs, see the Figure S11.

Supplementary figures and tables.

http://www.thno.org/v08p1923s1.pdf

Competing Interests

The authors have declared that no competing interest exists.

References

1. Ilic M, Ilic I. Epidemiology of pancreatic cancer. World J Gastroenterol. 2016; 22: 9694-9705.
2. Czito BG, Willett CG, Clark JW, Fernandez Del Castillo C. Current perspectives on locally advanced pancreatic cancer. Oncology. 2000; 14: 1535-45; discussion 46:49-52.
3. Li D, Xie K, Wolff R, Abbruzzese JL. Pancreatic cancer. Lancet. 2004; 363: 1049-1057.
4. Burris HA, 3rd, Moore MJ, Andersen J, Green MR, Rothenberg ML, Modiano MR, et al. Improvements in survival and clinical benefit with gemcitabine as first-line therapy for patients with advanced pancreas cancer: a randomized trial. J Clin Oncol. 1997; 15: 2403-2413.
5. Long J, Zhang Y, Yu X, Yang J, LeBrun DG, Chen C, et al. Overcoming drug resistance in pancreatic cancer. Expert Opin Ther Targets. 2011; 15: 817-828.
6. Freelove R, Walling AD. Pancreatic cancer: diagnosis and management. Am Fam Physician. 2006; 73: 485-492.
7. Neuzillet C, Tijeras-Raballand A, Bourget P, Cros J, Couvelard A, Sauvanet A, et al. State of the art and future directions of pancreatic ductal adenocarcinoma therapy. Pharmacol Ther. 2015; 155: 80-104.
8. Giovannetti E, Funel N, Peters GJ, Del Chiaro M, Erozenci LA, Vasile E, et al. MicroRNA-21 in pancreatic cancer: correlation with clinical outcome and pharmacologic aspects underlying its role in the modulation of gemcitabine activity. Cancer Res. 2010; 70: 4528-4538.
9. Rivera F, Lopez-Tarruella S, Vega-Villegas ME, Salcedo M. Treatment of advanced pancreatic cancer: from gemcitabine single agent to combinations and targeted therapy. Cancer Treat Rev. 2009; 35: 335-339.
10. Park JK, Lee EJ, Esau C, Schmittgen TD. Antisense inhibition of microRNA-21 or -221 arrests cell cycle, induces apoptosis, and sensitizes the effects of gemcitabine in pancreatic adenocarcinoma. Pancreas. 2009; 38: e190-199.
11. Passetti F, Ferreira CG, Costa FF. The impact of microRNAs and alternative splicing in pharmacogenomics. Pharmacogenomics J. 2009; 9: 1-13.
12. Iorio MV, Croce CM. MicroRNAs in cancer: small molecules with a huge impact. J Clin Oncol. 2009; 27: 5848-5856.
13. Blower PE, Chung JH, Verducci JS, Lin S, Park JK, Dai Z, et al. MicroRNAs modulate the chemosensitivity of tumor cells. Mol Cancer Ther. 2008; 7: 1-9.
14. Bloomston M, Frankel WL, Petrocca F, Volinia S, Alder H, Hagan JP, et al. MicroRNA expression patterns to differentiate pancreatic adenocarcinoma from normal pancreas and chronic pancreatitis. JAMA. 2007; 297: 1901-1908.
15. Aagaard L, Rossi JJ. RNAi therapeutics: principles, prospects and challenges. Adv Drug Deliv Rev. 2007; 59: 75-86.
16. Li Y, Sarkar FH. MicroRNA targeted therapeutic approach for pancreatic cancer. Int J Biol Sci. 2016; 12: 326-337.
17. Devulapally R, Foygel K, Sekar TV, Willmann JK, Paulmurugan R. Gemcitabine and Antisense-microRNA Co-encapsulated PLGA-PEG Polymer Nanoparticles for Hepatocellular Carcinoma Therapy. ACS Appl Mater Interfaces. 2016; 8: 33412-33422.
18. Devulapally R, Paulmurugan R. Polymer nanoparticles for drug and small silencing RNA delivery to treat cancers of different phenotypes. Wiley Interdiscip Rev Nanomed Nanobiotechnol. 2014; 6: 40-60.
19. Dutta T, Jain NK, McMillan NA, Parekh HS. Dendrimer nanocarriers as versatile vectors in gene delivery. Nanomedicine. 2010; 6: 25-34.
20. Kaneshiro TL, Lu ZR. Targeted intracellular codelivery of chemotherapeutics and nucleic acid with a well-defined dendrimer-based nanoglobular carrier. Biomaterials. 2009; 30: 5660-5666.
21. Qi R, Gao Y, Tang Y, He RR, Liu TL, He Y, et al. PEG-conjugated PAMAM dendrimers mediate efficient intramuscular gene expression. AAPS J. 2009; 11: 395-405.
22. Otsuka H, Nagasaki Y, Kataoka K. PEGylated nanoparticles for biological and pharmaceutical applications. Adv Drug Deliv Rev. 2003; 55: 403-419.
23. Xiao T, Hou W, Cao X, Wen S, Shen M, Shi X. Dendrimer-entrapped gold nanoparticles modified with folic acid for targeted gene delivery applications. Biomater Sci. 2013; 1: 1172-1180.
24. Qiu J, Kong L, Cao X, Li A, Tan H, Shi X. Dendrimer-entrapped gold nanoparticles modified with β-cyclodextrin for enhanced gene delivery applications. RSC Adv. 2016; 6: 25633-25640.
25. Shan Y, Luo T, Peng C, Sheng R, Cao A, Cao X, et al. Gene delivery using dendrimer-entrapped gold nanoparticles as nonviral vectors. Biomaterials. 2012; 33: 3025-3035.
26. Kong L, Alves CS, Hou W, Qiu J, Mohwald H, Tomas H, et al. RGD peptide-modified dendrimer-entrapped gold nanoparticles enable highly efficient and specific gene delivery to stem cells. ACS Appl Mater Interfaces. 2015; 7: 4833-4843.
27. Kong L, Wu Y, Alves CS, Shi X. Efficient delivery of therapeutic siRNA into glioblastoma cells using multifunctional dendrimer-entrapped gold nanoparticles. Nanomedicine. 2016; 11: 3103-3115.
28. Zhu J, Shi X. Dendrimer-based nanodevices for targeted drug delivery applications. J Mater Chem B. 2013; 1: 4199-4211.
29. Wang Y, Guo R, Cao X, Shen M, Shi X. Encapsulation of 2-methoxyestradiol within multifunctional poly(amidoamine) dendrimers for targeted cancer therapy. Biomaterials. 2011; 32: 3322--3329.
30. Fu F, Wu Y, Zhu J, Wen S, Shen M, Shi X. Multifunctional lactobionic acid-modified dendrimers for targeted drug delivery to liver cancer cells: investigating the role played by PEG spacer. ACS Appl Mater Interfaces. 2014; 6: 16416-16425.
31. Peng C, Zheng L, Chen Q, Shen M, Guo R, Wang H, et al. PEGylated dendrimer-entrapped gold nanoparticles for in vivo blood pool and tumor imaging by computed tomography. Biomaterials. 2012; 33: 1107-1119.
32. Santos JL, Oramas E, Pêgo AP, Granja PL, Tomás H. Osteogenic differentiation of mesenchymal stem cells using PAMAM dendrimers as gene delivery vectors. J Control Release. 2009; 134: 141-148.
33. Santos JL, Pandita D, Rodrigues J, Pêgo AP, Granja PL, Balian G, et al. Receptor-mediated gene delivery using PAMAM dendrimers conjugated with peptides recognized by mesenchymal stem cells. Mol Pharm. 2010; 7: 763-774.
34. Ren Y, Kang C-S, Yuan X-B, Zhou X, Xu P, Han L, et al. Co-delivery of as-miR-21 and 5-FU by poly (amidoamine) dendrimer attenuates human glioma cell growth in vitro. J Biomater Sci Polym Ed. 2010; 21: 303-314.
35. Lin LZ, Li F, Liu Y, Xing LX, Du LF. Contrast-Enhanced Ultrasound for differential diagnosis of pancreatic mass lesions: a meta-analysis. Med Ultrason. 2016; 18: 163-169.
36. Rickes S, Mönkemüller K, Malfertheiner P. Contrast-enhanced ultrasound in the diagnosis of pancreatic tumors. JOP. 2006; 7: 584-592.
37. Meijering BD, Juffermans LJ, van Wamel A, Henning RH, Zuhorn IS, Emmer M, et al. Ultrasound and microbubble-targeted delivery of macromolecules is regulated by induction of endocytosis and pore formation. Circ Res. 2009; 104: 679-687.
38. Arvanitis CD, Bazan-Peregrino M, Rifai B, Seymour LW, Coussios CC. Cavitation-enhanced extravasation for drug delivery. Ultrasound Med Biol. 2011; 37: 1838-1852.

39. Qiu Y, Luo Y, Zhang Y, Cui W, Zhang D, Wu J, et al. The correlation between acoustic cavitation and sonoporation involved in ultrasound-mediated DNA transfection with polyethylenimine (PEI) in vitro. J Control Release. 2010; 145: 40-48.

40. Wang T-Y, Choe JW, Pu K, Devulapally R, Bachawal S, Machtaler S, et al. Ultrasound-guided delivery of microRNA loaded nanoparticles into cancer. J Control Release. 2015; 203: 99-108.

41. Miller DL, Dou C. Induction of apoptosis in sonoporation and ultrasonic gene transfer. Ultrasound Med Biol. 2009; 35: 144-154.

42. Panje CM, Wang DS, Pysz MA, Paulmurugan R, Ren Y, Tranquart F, et al. Ultrasound-mediated gene delivery with cationic versus neutral microbubbles: effect of DNA and microbubble dose on in vivo transfection efficiency. Theranostics. 2012; 2: 1078-1091.

43. Lentacker I, De Cock I, Deckers R, De Smedt S, Moonen C. Understanding ultrasound induced sonoporation: definitions and underlying mechanisms. Adv Drug Deliv Rev. 2014; 72: 49-64.

44. Jin LF, Li F, Wang HP, Wei F, Qin P, Du LF. Ultrasound targeted microbubble destruction stimulates cellular endocytosis in facilitation of adeno-associated virus delivery. Int J Mol Sci. 2013; 14: 9737-9750.

45. Ma J, Xing LX, Shen M, Li F, Zhu MJ, Jin LF, et al. Ultrasound contrast-enhanced imaging and in vitro antitumor effect of paclitaxel-poly(lactic-co-glycolic acid)-monomethoxypoly (ethylene glycol) nanocapsules with ultrasound-targeted microbubble destruction. Mol Med Rep. 2015; 11: 2413-2420.

46. Xing L, Shi Q, Zheng K, Shen M, Ma J, Li F, et al. Ultrasound-Mediated Microbubble Destruction (UMMD) Facilitates the Delivery of CA19-9 Targeted and Paclitaxel Loaded mPEG-PLGA-PLL Nanoparticles in Pancreatic Cancer. Theranostics. 2016; 6: 1573-1587.

47. Majoros IJ, Williams CR, Baker J, James R. Current dendrimer applications in cancer diagnosis and therapy. Curr Top Med Chem. 2008; 8: 1165-1179.

48. Pandita D, Santos JL, Rodrigues J, Pêgo AP, Granja PL, Tomás H. Gene delivery into mesenchymal stem cells: a biomimetic approach using RGD nanoclusters based on poly (amidoamine) dendrimers. Biomacromolecules. 2011; 12: 472-481.

49. Chen Q, Li K, Wen S, Liu H, Peng C, Cai H, et al. Targeted CT/MR dual mode imaging of tumors using multifunctional dendrimer-entrapped gold nanoparticles. Biomaterials. 2013; 34: 5200-5209.

50. Peng C, Qin J, Zhou B, Chen Q, Shen M, Zhu M, et al. Targeted tumor CT imaging using folic acid-modified PEGylated dendrimer-entrapped gold nanoparticles. Polym Chem. 2013; 4: 4412-4424.

51. Lai C-Y, Wu C-H, Chen C-C, Li P-C. Quantitative relations of acoustic inertial cavitation with sonoporation and cell viability. Ultrasound Med Biol. 2006; 32: 1931-1941.

52. Yu H, Xu L. Cell experimental studies on sonoporation: state of the art and remaining problems. J Control Release. 2014; 174: 151-160.

53. Bader KB, Holland CK. Gauging the likelihood of stable cavitation from ultrasound contrast agents. Phys Med Biol. 2012; 58: 127-144.

54. Ren Y, Wang R, Gao L, Li K, Zhou X, Guo H, et al. Sequential co-delivery of miR-21 inhibitor followed by burst release doxorubicin using NIR-responsive hollow gold nanoparticle to enhance anticancer efficacy. J Control Release. 2016; 228: 74-86.

55. Qian X, Long L, Shi Z, Liu C, Qiu M, Sheng J, et al. Star-branched amphiphilic PLA-b-PDMAEMA copolymers for co-delivery of miR-21 inhibitor and doxorubicin to treat glioma. Biomaterials. 2014; 35: 2322-2335.

56. Xu L-f, Wu Z-p, Chen Y, Zhu Q-s, Hamidi S, Navab R. MicroRNA-21 (miR-21) regulates cellular proliferation, invasion, migration, and apoptosis by targeting PTEN, RECK and Bcl-2 in lung squamous carcinoma, Gejiu City, China. PloS one. 2014; 9: e103698.

57. Kaspar M, Partovi S, Aschwanden M, Imfeld S, Baldi T, Uthoff H, et al. Assessment of microcirculation by contrast-enhanced ultrasound: a new approach in vascular medicine. Swiss Med Wkly. 2015; 145: w14047.

58. Maeda H, Wu J, Sawa T, Matsumura Y, Hori K. Tumor vascular permeability and the EPR effect in macromolecular therapeutics: a review. J Control Release. 2000; 65: 271-284.

59. Aryal M, Park J, Vykhodtseva N, Zhang Y-Z, McDannold N. Enhancement in blood-tumor barrier permeability and delivery of liposomal doxorubicin using focused ultrasound and microbubbles: evaluation during tumor progression in a rat glioma model. Phys Med Biol. 2015; 60: 2511.

60. Yang Y, Bai W, Chen Y, Nan S, Lin Y, Ying T, et al. Low-frequency ultrasound-mediated microvessel disruption combined with docetaxel to treat prostate carcinoma xenografts in nude mice: A novel type of chemoembolization. Oncol Lett. 2016; 12: 1011-1018.

61. Ektate K, Kapoor A, Maples D, Tuysuzoglu A, VanOsdol J, Ramasami S, et al. Motion Compensated Ultrasound Imaging Allows Thermometry and Image Guided Drug Delivery Monitoring from Echogenic Liposomes. Theranostics. 2016; 6: 1963-1974.

62. Liu Y, Li F, Gao F, Xing L, Qin P, Liang X, et al. Periostin promotes tumor angiogenesis in pancreatic cancer via Erk/VEGF signaling. Oncotarget. 2016; 7: 40148-40159.